Fatigue Cracks in HVOF Thermally Sprayed WC-Co Coatings

S. Watanabe, T. Tajiri, N. Sakoda, and J. Amano

(Submitted 28 April 1997; in revised form 14 October 1997)

Initiation and early growth of fatigue cracks of a medium carbon steel with HVOF thermally sprayed WC-Co coatings prepared from two types of commercially available powders with similar total chemical composition were investigated under rotating bending conditions.

The morphology of the fatigue crack is divided into two type—linear cracks and net-like cracks—depending on the types of powders and the thickness of the coatings. The fatigue cracks in thinner coatings were closer to each other than those for the thick coatings.

1. Introduction

HVOF thermally sprayed WC-Co coatings with excellent wear-resistance properties have been widely used in aerospace, oil, and paper industries. The fatigue properties of these coatings are important in their practical application. However, there are few papers published on this subject (Ref 1-10). In particular, there is little information with respect to fatigue cracks in thermally sprayed WC-Co coatings.

The mechanism of initiation and early growth of fatigue cracks in a HVOF thermally sprayed WC-12wt%Co coating was studied. Attention is given to the adhesion of deposited particles and the nature of the interface between the coating and the substrate and to the morphology of the crack path in the coatings.

2. Experimental Procedures

The material used as a substrate was a medium carbon steel having a chemical composition (wt%) of 0.43%C, 0.21%Si,

S. Watanabe and **J. Amano,** Matue National College of Technology, 14-4, Nishiikuma-cho, Matue-shi, Shimane 690, Japan; **T. Tajiri** and **N. Sakoda,** Kurashiki Boring Kiko Co., Ltd., 4-20, Matue 2 chome, Kurashiki-shi, Okayama 712, Japan.

0.66%Mn, 0.018%P, 0.008%S, 0.13%Cu, 0.09%Ni, 0.20%Cr, with the balance being iron. Figure 1 indicates the dimensions of the rod specimen. All specimens were annealed for 0.5 h in a vacuum of 5×10^{-4} Pa at 1123 K. The surfaces of specimens (shaded region in Fig. 1) were subjected to grit blasting with Al_2O_3 grit at a pressure of 0.5 MPa. Two types of commercially available WC-12wt%Co powders, each manufactured by a different process, were considered for HVOF spraying. These powder types and manufacturing processes were type A, cast and crushed; and type B, agglomerated and sintered.

The spray parameters are indicated in Table 1. As-sprayed coatings were 75 ± 10 µm and 125 ± 10 µm in thickness, and then they were ground with a diamond wheel to 50 ± 10 µm and 100 ± 10 µm, respectively. The coated specimens were subjected to fatigue tests on a rotating bending machine at a frequency of 36 Hz. Some of the specimens were polished with diamond paste to 1 µm before the fatigue test to specifically examine crack behavior. The stress amplitudes were calculated using the substrate specimen diameter. Examination of the fatigued specimen surfaces was performed by optical microscopy and scanning electron microscopy (SEM).

Table 1 Thermal spraying parameters

Spraying apparatus	HVOF (DJ)
Fuel pressure (C_3H_6)	0.7 MPa
Oxygen pressure (O_2)	1.0 MPa
Powder feed gas pressure (N_2)	0.9 MPa
Spraying distance	185 mm
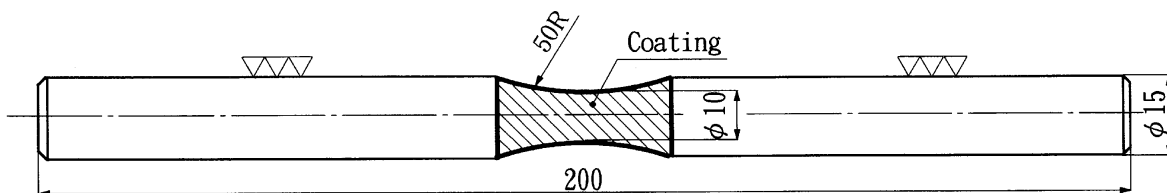
Fig. 1 Size and dimensions of rod specimens. All dimensions recorded in millimeters.

3. Results and Discussion

Figure 2 shows the S-N diagrams of the coated specimens. The fatigue limits of the coated specimens and the grit blasted ones show clearly higher values compared to the annealed specimens. Also, the fatigue limits of the coated specimens are almost the same as 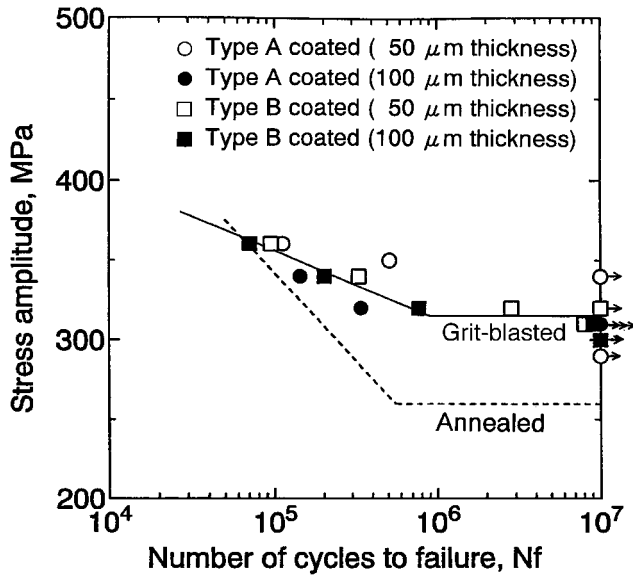or higher than that of the grit blasted specimens. For the type A coated specimens, the fatigue limit of the specimens with a 50 μm coating are higher than that of the specimens with a 100 μm coating. For the type B coated specimens, the fatigue limit of the specimens with a 50 μm coating is approximately equal to that of the specimens with a 100 μm coating, but at the higher stress level the fatigue life of the former is greater. It can be noted that the effect of coating thickness on fatigue limit is affected by coating thickness for type A powder coated specimen, but the influence for the type B powder coated specimen is less significant.

Figure 3 shows a typical example of the fatigue cracks in each coated specimen. The type A coated specimen with 50 μm coating was tested at a stress of 350 MPa, and the others were tested at a stress of 320 MPa. The morphology of fatigue cracks in the type A coating is different from that in the type B coating. The type A coating produces linear cracks, and the type B coating produces net-like cracks. Also, for both coatings the number of cracks in the thinner coating layer are more than that in the thicker coating layer.

Figure 4 is an SEM photograph of the surface of type A coated specimens. Figure 4(a) shows deformation on the specimen surface with a 50 μm thick coating which is at right angles to the loading axis with no crack formation. After 2×10^5 cycles, such features were not found on the surface. Therefore, this feature indicates the deformation by internal fatigue crack propagation. Such deformation was not found on the surfaces of the other coated specimens tested at a stress of 320 MPa. This fact indicates that the specimen has good cohesion between particles and good adhesion at the interface between the coating and the
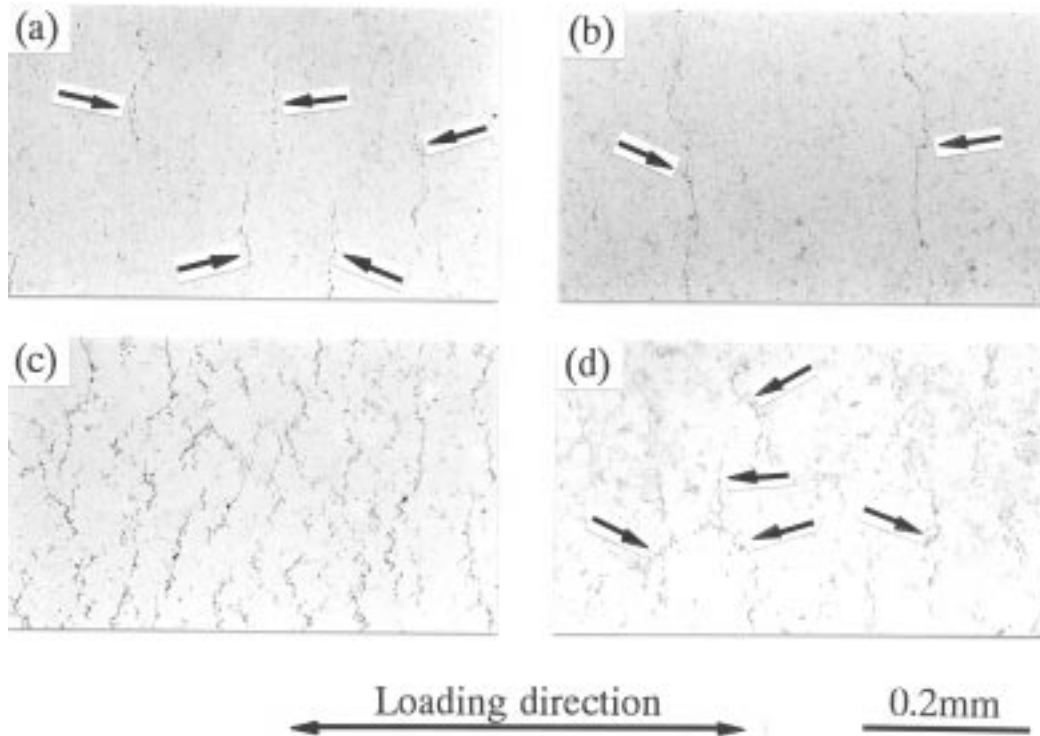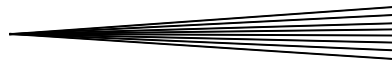

Fig. 2 S-N diagram of thermally sprayed specimens

Fig. 3 Typical examples of fatigue cracks in coatings. (a) Type A coated (50 μm thick coating), σ = 350 MPa, $N = 2 \times 10^5$. (b) Type A coated (100 μm thick coating), σ = 320 MPa, $N = 10^4$. (c) Type B coated (50 μm thick coating), σ = 320 MPa, $N = 10^5$. (d) Type B coated (100 μm thick coating), σ = 320 MPa, $N = 10^5$

substrate. Figure 4(b) shows the fatigue cracks on the surface of a specimen with a 100 μm coating. The cracks are narrow, and the crack tips are sharp. Also, the fatigue crack propagated around the specimen perimeter at an early stage. These observa-

Loading direction
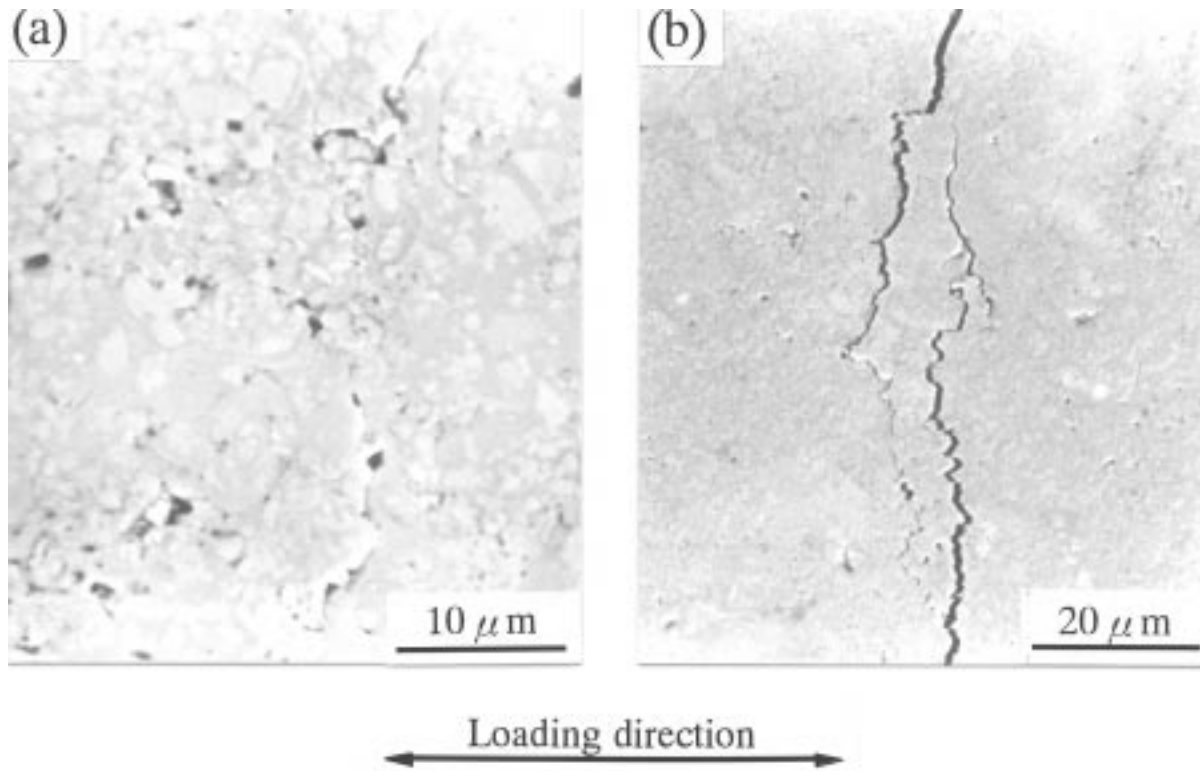
Fig. 4 SEM photographs of fatigue cracks in the type A coatings. (a) 50 μm thick coating, $\sigma = 350$ MPa, $N = 2 \times 10^4$. (b) 100 μm thick coating, $\sigma = 320$ MPa, $N = 10^4$

Loading direction
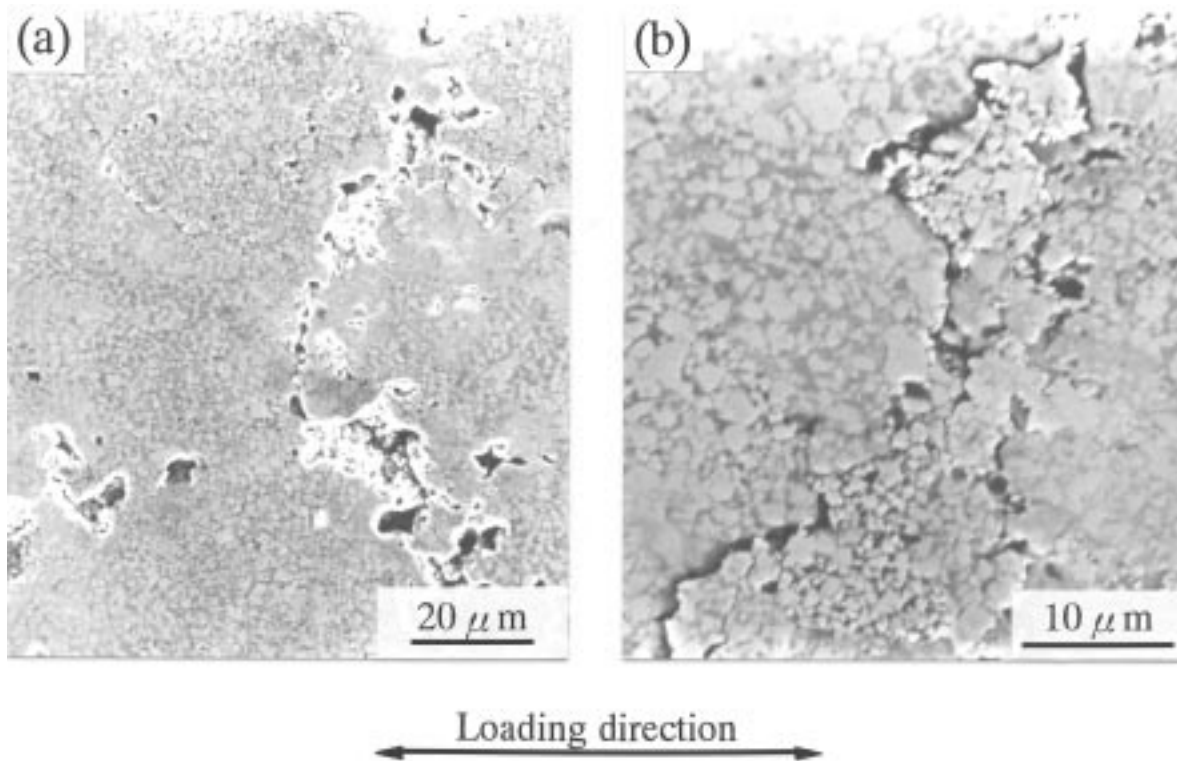
Fig. 5 SEM photographs of fatigue cracks in the type B coatings. (a) 50 μm thick coating, $\sigma = 320$ MPa, $N = 10^7$. (b) 100 μm thick coating, $\sigma = 320$ MPa, $N = 7 \times 10^5$

tions indicate that the specimen exhibited good cohesion between particles, but poor adhesion of the interface between the coating and the substrate relative to the specimen with 50 μm coating. Such difference in the adhesion of the interface between the coating and the substrate for these two specimens influences the number of the fatigue cracks in coatings.

The type B coated specimens exhibited fatigue cracks as shown in Fig. 5 for both the 50 μm and the 100 μm thick coatings. Figure 5(a) shows an example of fatigue cracks originating at the triple points of deposited particles. Figure 5(b) indicates fatigue cracks originating at the boundary of unmelted particles. The existence of such unmelted particles in the coating will offer poor adhesion and promote crack initiation under a stress field. These cracks are responsible for the net-like cracks when they join during fatigue initiation, Fig. 3(c) and (d). Therefore, the type B coated specimens have poor cohesion between particles and poor adhesion at the interface between the coating and the substrate. As a result, the effect of coating thickness on the fatigue strength is less prominent, although the effect of coating thickness on the number of fatigue cracks appears to be a sensitive parameter. This phenomenon is the same for type A coated specimens. Therefore, it is considered that the adhesion strength for type B coated specimens will also decrease with increasing coating thickness. In this case, when a load is applied to a coated specimen, a crack is at first initiated at the interface between the coating and the substrate, resulting in the suppression of other cracks in the coating because of stress relief. Hence, it is concluded that the difference in the number of fatigue cracks between the thinner and thicker coating reflects a bonding state at the interface between the coating and the substrate.

4. Conclusions

The morphology of fatigue cracks in coatings is dominated by the bonding state at the interface of deposited particles and at the interface between the coating and the substrate. This has been shown in practice to be an efficient way to evaluate thermal sprayed coatings.

References

1. H.D. Steffens, R. Dammer, and U. Fischer, Influence of Sprayed Metal Coatings on the Behavior of Components under Dynamic Loading, *Advances in Thermal Spraying,* The Welding Institute of Canada, 1986, p 417-425

2. O. Knotek, R. Elsing, and H.R. Heintz, "On the Microstructure and Properties of Plasma-Sprayed Wsi2 Coatings, Advances in Thermal Spraying," *Advances in Thermal Spraying,* The Welding Institute of Canada, 1986, p 427-433

3. E. Lugscheider, R. Mathesius, G. Spur, and A. Kranz, Mechanical Properties of Thermal Sprayed Coatings on CFRP, *Thermal Spray Coatings: Research, Design, and Applications,* C.C. Berndt and T.F. Bernecki, Ed., ASM International, 1993, p 569-573

4. J. Wigren, L. Pejryd, D.J. Greving, J.R. Shadley, and E.F. Rybicki, Performance Evaluations and Selection of Tungsten Carbide Thermal Spray Coatings for Mid-Span Dampers, *Thermal Spraying: Current Status and Future Trends,* A. Ohmori, Ed., High Temperature Society of Japan (Osaka), 1995, p 113-118

5. M. Sugano, H. Masaki, J. Kishimoto, Y. Nasu, and T Satake, A Microstructural Study of Fatigue Damage in Stainless Steel Coated with Plasma-Sprayed Alumina, *Thermal Spraying: Current Status and Future Trends,* A. Ohmori, Ed., High Temperature Society of Japan (Osaka), 1995, p 145-150

6. J.U. Hwangm, T. Ogawa, and K. Tokaji, Fatigue Strength and Fracture Mechanisms of Ceramic-Sprayed Steel in Air and a Corrosive Environment, *Thermal Spraying: Current Status and Future Trends,* A. Ohmori, Ed., High Temperature Society of Japan (Osaka), 1995, p 767-772

7. T. Shiraishi, H. Ogiyama, and H. Tshkuda, Effect of Thermal Sprayed Ceramic Coatings on Fatigue Behavior of Metals, *Thermal Spraying: Current Status and Future Trends,* A. Ohmori, Ed., High Temperature Society of Japan (Osaka), 1995, p 845-850

8. M. Hadfield, R. Ahmed, and S. Tobe, Rolling Contact Fatigue of Thermal Spray Coated Cones, *Thermal Spraying: Current Status and Future Trends,* A. Ohmori, Ed., High Temperature Society of Japan (Osaka), 1995, p 1097-1102

9. O.C. Brandt, Mechanical Properties of HVOF Coating, *J. Thermal Spray Technol.,* Vol 4 (No. 2), 1995, p 147-152

10. K. Tokaji, T. Ogawa, J.U. Hwang, Y. Kobayashi, and Y. Harada, Corrosion Fatigue Behavior of a Steel with Sprayed Coatings, *J. Thermal Spray Technol.,* Vol 5 (No. 3), 1996, p 269-276